Project Report on
"Experimental Study of Thermal Pressurization and the Role of Fault Roughness"

INTRODUCTION

We have been studying the widely discussed dynamic weakening mechanism termed *thermal pore-fluid pressurization*. There are many theoretical and numerical studies of thermal pressurization [*Andrews*, 2002; *Lachenbruch*, 1980; *Lee and Delaney*, 1987; *Mase and Smith*, 1985; 1987; *Noda*, 2008; *Noda and Shimamoto*, 2005; *Rempel and Rice*, 2006; *Rice*, 2006; *Rice and Cocco*, 2007; *Sibson*, 1973] and it is increasingly used in dynamic rupture and earthquake nucleation models [*Bizzarri and Cocco*, 2006a; b; *Lapusta and Rice*, 2004a; b; *Noda et al.*, 2009; *Noda and Lapusta*, 2010; *Rice et al.*, 2010; *Schmitt and Segall*, 2009; *Segall and Rice*, 2006]. Our experiment studies of thermal pressurization are the most definitive ones yet obtained.

This project is a continuation of the work funded in our current proposal of the same title. With SCEC 2019 funding we continued experiments to further investigate fault-weakening via thermal pore-fluid pressurization. Consequently, this first overview portion of this proposal repeats some of what we have written in previous years so that reviewers who did not read previous versions will be adequately informed of the necessary background.

Part of our emphasis has been on trying to understand the role that fault-roughness-induced dilatancy may play in defeating this weakening mechanism on natural faults. We have heretofore demonstrated that thermal pressurization weakening occurs in our experiments on flat, but slightly roughened faults. However, both the theoretical and experimental results apply to flat surfaces, whereas natural faults have a self-affine, approximately self-similar roughness, which is characterized by an amplitude-to-wavelength ratio of 10^{-3} to 10^{-2} in the slip direction *[Power and Tullis, 1991; 1995; Power et al., 1987; Power et al., 1988; Sagy et al*., 2007; *Candela et al.,* 2012; *Thom et al.,* 2017; *Brodsky et al*., 2011, 2016]. Furthermore natural faults with this roughness are mated together across these surfaces [*Power and Tullis*, 1992]. This means that when faults slip, the roughness either becomes unmated or is accommodated by elastic and inelastic deformation. Accommodation, either by opening of the surfaces as would occur if the wall rocks were rigid, or by inelastic brittle deformation, or both, will result in dilatancy. Depending on the relative magnitude of the pore-volume increase and the volume increase of the thermally expanding pore fluid, the net effect on the pore pressure may either be a increase in pore pressure smaller than in the absence of dilatancy, or a reduction in pore pressure. In the latter case dilatancy hardening [*Lockner and Byerlee*, 1994] would occur rather than thermal pressurization weakening. All of the theoretical work on thermal pressurization weakening, as well as our continued experimental study of this process, will have no applicability to slip during earthquakes if a factor not included in those studies completely obliterates the weakening.

It is important to note that due to the approximately self-similar character of fault roughness, the dilatancy it produces will continue to become progressively larger as slip continues. This is because as more slip occurs the longer wavelength bumps that become unmated have higher amplitudes. Thus, this dilatancy is unlike a transient dilatancy due to a change in slip velocity that also occurs [*Beeler and Tullis*, 1997; *Lockner and Byerlee*, 1994; *Marone et al.*, 1990]. This transient dilatancy occurs at the onset of more rapid slip and is taken into account by the analysis of [*Rice*, 2006; *Segall and Rice*, 1995; 2006]. However, although *Rice* [2006] considers some effects that inelastic dilatancy may have on the properties of the near-fault material, none of the many theoretical and numerical studies of thermal pressurization weakening address the important issue of progressive dilatancy with continued slip.

The greatest dilatancy produced by sliding on initially mated rough surfaces of course occurs if all the accommodation occurs by normal opening as would be the case if the rocks were rigid. However, considerable dilatancy also occurs as a result of brittle failure and cataclastic flow. The particles produced by these processes do not fit together nearly as well as they did before the deformation occurred. Even though small particles can fit between larger ones, considerable void space is created between the fragments

and this will produce suction on the pore fluid. How much dilatancy results from this process is unclear and remains to be determined by experiment.

As described in last year's proposal, we had been frustrated to find that thermal pressurization weakening occurred in some experiments but not in others. This made us think that some uncontrolled variable was responsible for the inconsistent results and suspected that leaks were occurring along the epoxy at the rock-steel interface. During the initial part of this past year's research we have verified that this is the case, and have found a better epoxy and have found thermal pressurization weakening in every experiment on smooth surfaces. The results in Figs. 1, 2, and 3 below document this weakening and the correlation of its character with the measured permeability of the samples and summarize portions of a paper now in press in JGR [*Badt et al.*, 2020]. Following that are new results on an initially mated rough surface, similar to the experiment we reported on two years ago, except that the new experiment has a much wider range of wavelengths in its roughness.

RESULTS

Permeability of Fredrick Diabase. Plots of permeability versus effective confining pressure are illustrated for selected samples in Fig. 1. The permeability was estimated primarily using constant pressure-difference, flow-through experiments (samples 340, 346, and 352); permeability for sample 340 was also estimated by the pore pressure oscillation method at effective confining pressures 7 and 20 MPa. Samples 340 and 344 underwent the same heat treatment at 630°C, while sample 346 was heat treated to 530°C. Accordingly, the permeability of sample 346 was ~1 order of magnitude lower than the other two samples. Sample 352 exhibited a higher permeability than sample 340, even though they were heat treated to the same temperature, but for different durations – 340 for 1 hour at peak temperature; 352 for 4 hours at peak temperature. The difference in permeability for samples 340 and 352 may be attributed to time-dependent sub-critical crack growth at elevated temperatures [*Fredrich and Wong, 1986; Martin, 1992].*

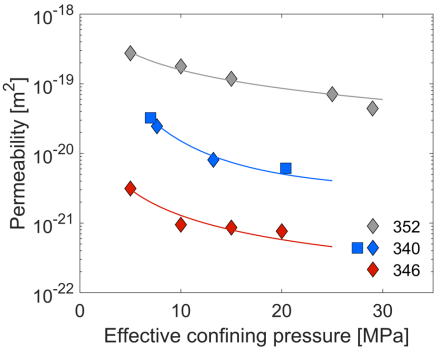

Figure 1. Permeability results compilation for heat-treated samples. The data are fitted by a power law in the form of $\boldsymbol{k = aP_c^b + c}$, where $\boldsymbol{P_c}$ is the effective confining pressure and $\boldsymbol{a}$, $\boldsymbol{b}$, and $\boldsymbol{c}$ are constants. Sample 340 and 352 were heat treated to **630**°C for 1 and 4 hours, respectively, while sample 346 was heat treated to **530**°C for 1 hour. Diamonds depict flow-through estimates, squares (available only for 340) depict pore pressure oscillation estimate.

Dry Friction. The dry (sample prepared at room humidity of 35%) frictional response is illustrated in Fig.2 for velocity step-ups from a reference velocity v_0=3.162 μm/s to v=2.5 mm/s (a) and v=5 mm/s (b) and then back down to the reference velocity. These data show velocity-strengthening behavior, with an increase in friction at the step-up, after which friction remains elevated relative to friction at the reference velocity, without an obvious evolution effect Namely, the frictional behavior can be fit by a logarithmic law involving only the "direct effect" in rate-and -state friction.

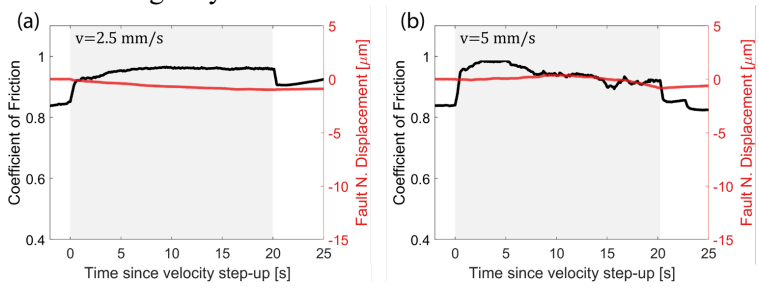

Figure 2. Dry frictional evolution and fault normal displacement (negative=dilation; positive=compaction) during a velocity step, from reference velocity $\boldsymbol{v_0}$=3.162 μm (unshaded areas) to high velocity $\boldsymbol{v}$ (shaded areas); (a) $\boldsymbol{v}$=2.5 mm/s, (b) $\boldsymbol{v}$=5 mm/s. Fault normal displacement accounts for $\boldsymbol{< 1\ \mu m}$ during a velocity step with little change in the step up ($\boldsymbol{v_0 \rightarrow v}$) or the step down ($\boldsymbol{v \rightarrow v_0}$).

Friction of water-saturated, low permeability samples. The evolution of friction for water-saturated, low permeability faults is illustrated for three different samples in Fig. 3 for velocity steps from v_0 to v=2.5 mm/s, then back to v_0. These data differ significantly from the dry (Fig. 2) case. At the velocity step-up,

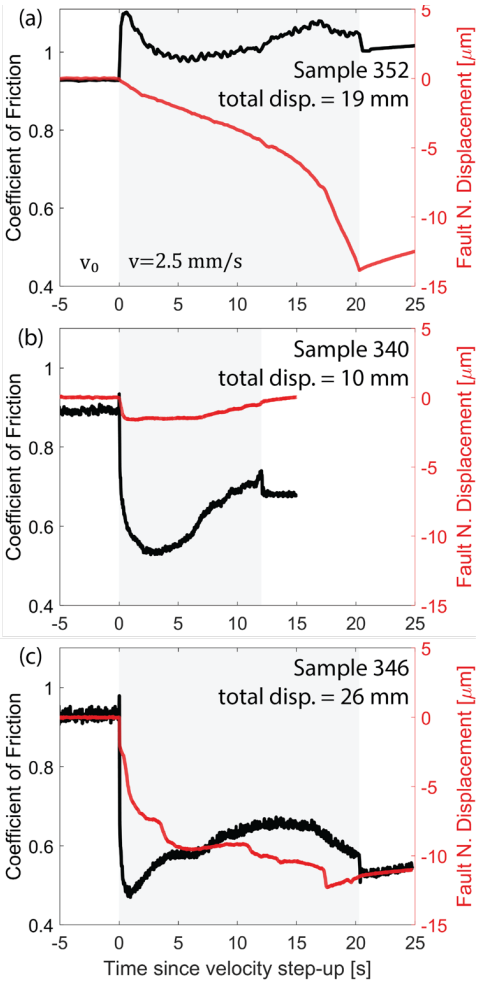

Figure 3. Friction and fault normal displacement during a velocity step from reference velocity $\boldsymbol{v_0 = 3.162\ \mu m/s}$ to $\boldsymbol{v = 2.5\ mm/s}$, for samples 352 (a), 340 (b) and 346 (c). A transient increase in friction is observed during the step up, followed by weakening. Dilatancy is observed at the velocity step up and during weakening. Strengthening of the fault follows the weakening phase, which is associated with both dilation (352 and 346) and compaction (340). Total displacement at the time of the velocity step-up is given under the sample ID.

friction increases as in the dry experiment, however, this increase is followed by weakening, where the friction drops from the peak value by 12%, 43% and 52%, for samples 352, 340 and 346, respectively (Fig. 3). The maximum rate of weakening scales with the magnitude of weakening in these experiments; weakening rates of 1.4 MPa/mm, 14 MPa/mm and 27 MPa/mm are calculated for samples 352, 340 and 346, respectively. Dynamic weakening is not maintained throughout the entire course of the high velocity interval; friction increases gradually after the initial stage of weakening. Sample 346 (Fig 3c) exhibits a faster transition from weakening to strengthening, compared to samples 352 and 340, and a subsequent weakening event during the final stages of the velocity step that is also observed in sample 352. Note that the duration of fast-slip is shorter for sample 340 (12 seconds – 30 mm) compared to samples 346 and 352 (20 seconds – 50 mm). Samples 340 and 346 were subjected to an effective normal stress of σ_n^{eff}=25 MPa, effective confining pressure of P_c^{eff}=25 MPa, while for sample 352 these were σ_n^{eff}=50 MPa and P_c^{eff}=49 MPa. As noted above, these samples underwent different heat treatment and thus their permeabilities (k) were different, with $k_{352} > k_{340} > k_{346}$ (Fig.1). The fault normal displacement at water-saturated conditions also differs significantly from that observed at dry conditions (Fig 2). All of the water-saturated samples display transient dilation after the change in velocity and the onset of frictional weakening, although their behavior differs from one another (Fig. 3).

New results on an initially mated rough surface. We have generated a second pair of mated samples with the same amplitude to wavelength ratios of 0.0014 as we used two years ago, but with 9 self-similar wavelengths rather than only 2. As before, these surfaces were generated with our CNC milling machine and subsequently sandblasted to produce additional finer-scale roughness. The experimental results from this sample pair are quite interesting although they raise questions that we can only answer by further experiments that will be undertaken during our 2020 grant.

The results are shown in Fig. 4 which is complicated enough that it requires careful examination. Some of what is seen is expected, whereas some is puzzling. A variety of parameters are plotted versus slip distance for one revolution of our rotary shear sample which is 154.6 mm. In solid green we show what the dilatancy would be if the samples were rigid and move apart while remaining coaxial. Given that the stresses are significant we would expect less dilatancy because some of the roughness should be destroyed by cataclastic deformation. Indeed, we found this to be the case in our 2-wavelength sample two years ago. Rigid sample behavior then predicted 0.53 mm of opening and we observed only 0.11 mm. As the solid green curve in Fig. 4 shows, for our 9-wavelength sample, rigid behavior predicts 0.65 mm of opening. In contrast we observe 0.19 mm (dark blue curve labeled 1st revolution). The expected and observed variation in dilatancy with slip are similar in shape but not in amplitude, if the observed curve is not perturbed by time-dependent compaction. This is shown by comparing the labeled light blue curve of observed dilatancy for the 2nd revolution done at constant velocity (down-shifted to start at zero dilatancy)

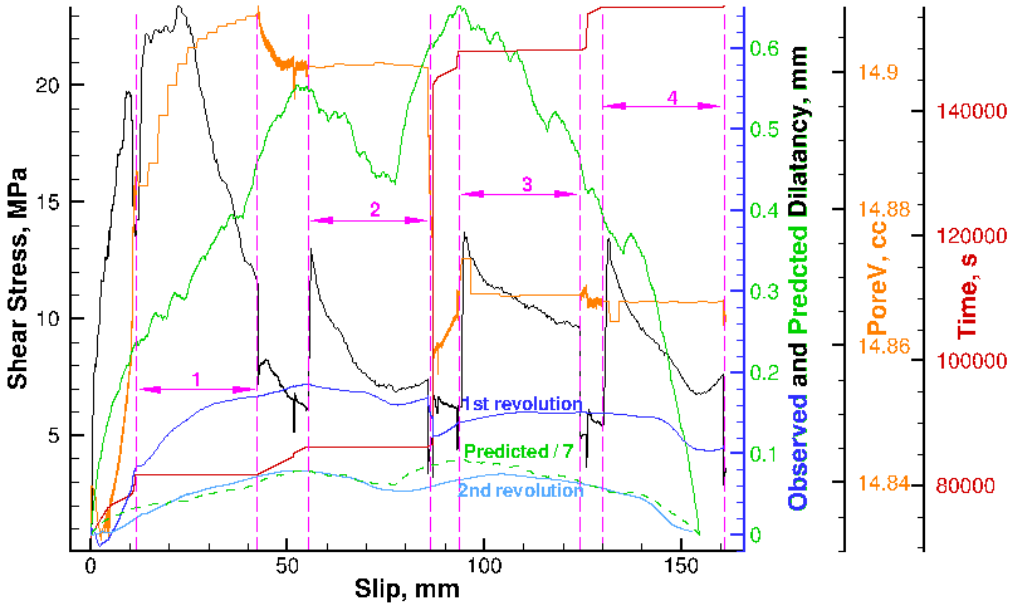

Figure 4. Results of an experiment on rough mated surfaces with 9 wavelengths, each having an amplitude to wavelength ratio of 0.0014. The sample has the same permeability and the conditions of the experiment were the same as for experiment 340. See text for discussion of the various curves and the implications of the results.

with the dashed green curve which is the predicted dilatancy divided by 7. In both experiments there is some permanent dilatancy after one sample revolution which presumably results from cataclastic debris filling in some of the space and consequently prevents the samples from being able to mate after one revolution. The amplitude of this permanent dilation is 0.09 mm in our first sample and 0.11 mm in the one shown in Fig. 4. Given this measured dilatancy, both the permanent part and the part that varies with displacement, our initial expectations that thermal pressurization might be prevented from occurring would seem likely. However, our observations are ambiguous with respect to this as is now discussed.

Fig. 4 shows four intervals, marked with magenta arrows, where we stepped the speed up from 3.2 μm/s to 2.5 mm/s. As Figure 3b shows for a flat sample with the same permeability, this velocity step under the same conditions of confining pressure, normal stress, and initial pore pressure would show a rapid shear stress decrease of about 40 percent. What we see in Figure 4 is similar to what we saw in our first sample two years ago, namely a larger stress decrease of about 70 percent during the first high-speed step and then smaller decreases after the others. This weakening may be due to thermal pressurization, although, as we now discuss, the evidence is contradictory.

The interpretation that thermal pressurization may have caused the large weakening during the first high speed sliding is supported by the behavior of the actuator that controls the pore pressure at the outer end of the sample. Even with a permeability of about 10^{-20} m^2 for this sample as for sample 340 (Fig. 1), the increases or decreases in pressure on the fault surface result in fluid either flowing out of or into the sample, respectively, because our servo system keeps the pressure on the outer end of the sample constant. As the fault dilates both before and during the first high velocity interval the fluid flows into the sample as indicated by the increase in the "pore volume" going into the sample (Fig. 4, orange curve). This can only occur if the pore pressure on the fault is decreasing and so more fluid is needed to try to keep the fault's pore pressure constant. Perhaps the even larger decrease in shear stress seen in this experiment than in sample 340 shown in Fig. 3b could be due to a larger volume of water to be heated along the fault in this rough surface, given that about 50 mm^3 of water was drawn in during the dilatancy that occurred while the sample slipped from about 5 to 11 mm prior to the first high speed step.

The subsequent pore volume data suggest that the pore pressure increased during the last half of that first high-speed sliding interval, presumably due to thermal pressurization. The relevant intriguing observation is that during the interval of slow sliding between the first and second fast sliding intervals the pore volume curve shows that fluid is flowing out of the sample, indicating that the pore pressure on the fault is higher

than the controlled value at the outer end of the sample. Furthermore, the fluid is flowing out even though the sample is continuing to dilate, which by itself would cause fluid to flow in.

However, there is a good argument against thermal pressurization causing the reduction in shear stress from 23 to 12 MPa during the first high-speed step. If that were the case, once the pore pressure on the fault returned to the initial value being maintained on the outer end of the sample, the strength should have returned to its initial value, but it never did, whereas it does for thermal pressurization on our flat samples [*Badt et al*., 2020]. Even after the sample sat overnight for about 16 hours (see change in time at 86 mm on the slip axis) it never re-strengthened although it is evident that the pore pressure had come to equilibrium because flow had stopped. This suggests that the large permanent decrease in shear stress may be due to some mechanism related to the mated roughness of the sample or to some experimental artifact and have nothing to do with fluid pressure. For example, if the Teflon rings that separate the O-rings from the sample were too large in the axial direction, then they could possibly be carrying some of the normal stress that we assume is borne by the sample. We tried to make them extra short to eliminate that possibility. The fact that they were not in contact at the beginning of the experiment and that a net dilation occurs argues that the Teflon cannot be the problem, but we need to verify the situation. One way to determine whether fluid is playing any role is to use similarly rough mated dry samples and discover if the large permanent weakening still occurs.

One other puzzling feature of the shear stress record in Fig. 4 is that there are larger than expected increases in shear stress when the velocity increases, whether within the μm/s range or during the increase to 2.5 mm/s. They are much larger than one would expect for the direct effect in rate and state friction as can be seen by comparison with that response in Figures 2 and 3. It is possible that it is all due to dilatant hardening, the increase in the effective normal stress when pore pressure drops, although the lack of a dilatant signal when the shear stress increases occur, e.g. at 55, 94 and 130 mm of slip, argues against this. Again, it would be interesting to see if this large velocity effect exists in dry mated rough samples.

DISCUSSION

Our experimental results show that thermal pressurization does occur. However, as discussed in last year's report, and illustrated in Figure 3, an unexpected strengthening sometimes occurs following the initial weakening. As discussed in last year's report, this suggests that existing theoretical treatments of thermal pressurization [e.g. *Rice,* 2006] may neglect some important factors that can alter the results from those expected. In particular our results suggest that the expected increase in fluid pressure during thermal pressurization will increase the pore fluid diffusivity and, at least for our experimental geometry, may cause structural damage due to development of tensile stresses in the fault. Our calculations show that these structural and hydraulic changes may be responsible for inhibiting further weakening and may even reduce the fluid pressure and thereby promote frictional strengthening as observed in our experimental faults.

Furthermore, as our experiments on surfaces with initially realistic roughness characteristics show, the behavior differs from that seen for initially flat surfaces. It is too early in our study of these rough surfaces to be able to characterize their behavior. Our initial expectation is that thermal pressurization weakening will be decreased, but the results of the two initial experiments show unexpected weakening which may or may not be due to thermal pressurization. We hope that the series of experiments we have recently been funded to do as a continuation of this project will allow us to understand the role that fault roughness may play on thermal pressurization weakening and consequently make it more clear whether this weakening mechanism is a viable one to use in understanding dynamic weakening during earthquakes.

REFERENCES CITED

Andrews, D. J. (2002), A fault constitutive relation accounting for thermal pressurization of pore fluid, *J. Geophys. Res.*, *107*, 12.

Badt, N. Z., Tullis, T. E., & Hirth, G. (2020). Thermal pressurization weakening in laboratory experiments. *Journal of Geophysical Research: Solid Earth. in press.*

Beeler, N. M., and T. E. Tullis (1997), The roles of time and displacement in velocity-dependent volumetric strain of faults, *J. Geophys. Res.*, *102*, 22595-22609.

Bizzarri, A., and M. Cocco (2006a), A thermal pressurization model for the spontaneous dynamic rupture propagation on a three-dimensional fault: 1. Methodological approach, *J. Geophys. Res.*, *111*, B05303, doi:05310.01029/02005JB003862.

Bizzarri, A., and M. Cocco (2006b), A thermal pressurization model for the spontaneous dynamic rupture propagation on a three-dimensional fault: 2. Traction evolution and dynamic parameters, *J. Geophys. Res.*, *111*, B05304, doi:05310.01029/02005JB003864.

Brodsky, E. E., J. G. Jacquelyn, S. Amir, and C. Cristiano (2011), Faults smooth gradually as a function of slip, *Earth Planet. Sci. Lett.*, *302*, 185-193.

Brodsky, E. E., J. D. Kirkpatrick, and T. Candela (2016), Constraints from fault roughness on the scale-dependent strength of rocks, *Geology*, *44*, 19-22. doi:10.1130/G37206.37201.

Candela, T., F. Renard, Y. Klinger, K. Mair, J. Schmittbuhl, and E. E. Brodsky (2012), Roughness of fault surfaces over nine decades of length scales, J. Geophys. Res. Solid Earth, 117, B08409. doi:08410.01029/02011JB009041.

Fredrich, J. T., and T.-f. Wong (1986), Micromechanics of thermally induced cracking in three crustal rocks, *J. Geophys. Res.*, *91*, 12,743-712,764.

Lachenbruch, A. H. (1980), Frictional heating, fluid pressure, and the resistance to fault motion, *J. Geophys. Res.*, *85*, 6249-6272.

Lapusta, N., and J. R. Rice (2004a), Earthquake sequences on rate and state faults with strong dynamic weakening, paper presented at 2004 SCEC Annual Meeting Proceedings and Abstracts, Southern California Earthquake Center, PalmSprings, California, 2004.

Lapusta, N., and J. R. Rice (2004b), Earthquake sequences on rate and state faults with strong dynamic weakening, *Eos. Trans. Am. Geophys. Union, Fall Meeting Suppl.*, *85*(47), T22A-05.

Lee, T. C., and P. T. Delaney (1987), Frictional Heating and Pore Pressure Rise Due to a Fault Slip, *Geophysical Journal of the Royal Astronomical Society*, *88*(3), 569-591.

Lockner, D. A., and J. D. Byerlee (1994), Dilatancy in hydraulically isolated fault and the suppression of instability, *Geophys. Res. Lett.*, *21*, 2353-2356.

Marone, C. J., C. B. Raleigh, and C. H. Scholz (1990), Frictional behavior and constitutive modeling of simulated fault gouge, *J. Geophys. Res.*, *95*, 7007-7025.

Martin III, R. J. (1972). Time-dependent crack growth in quartz and its application to the creep of rocks. *Journal of Geophysical Research, 77*(8), 1406-1419.

Mase, C. W., and L. Smith (1985), Pore-fluid pressures and frictional heating on a fault surface, *Pure Appl. Geophys.*, *122*, 583-607.

Mase, C. W., and L. Smith (1987), Effects of frictional heating on the thermal hydrologic and mechanical response of a fault, *J. Geophys. Res.*, *92*, 6249-6272.

Noda, H. (2008), Frictional constitutive law at intermediate slip rates accounting for flash heating and thermally activated slip process, *J. Geophys. Res.*, doi:10.1029/2007JB005406.

Noda, H., E. M. Dunham, and J. R. Rice (2009), Earthquake ruptures with thermal weakening and the operation of major faults at low overall stress levels, *J. Geophys. Res.*, *114 (B07302)*, doi:10.1029/2008JB006143.

Noda, H., and N. Lapusta (2010), Three-dimensional earthquake sequence simulations with evolving temperature and pore pressure due to shear heating: Effect of heterogeneous hydraulic diffusivity, *J. Geophys. Res.*, *115*, B12314.

Noda, H., and T. Shimamoto (2005), Thermal pressurization and slip-weakening distance of a fault: An example of the Hanaore fault, southwest Japan, *Bull. Seis. Soc. Am.*, *95*(4), 1224-1233.

Power, W. L., and T. E. Tullis (1991), Euclidian and fractal models for the description of rock surface roughness, *J. Geophys. Res*, *96*, 415-424.

Power, W. L., and T. E. Tullis (1992), The contact between opposing fault surfaces at Dixie Valley, Nevada, and implications for fault mechanics, *J. Geophys. Res.*, *97*, 15425-15435.

Power, W. L., and T. E. Tullis (1995), A review of the fractal character of natural fault surfaces with implications for friction and the evolution of fault zones, in *Fractals in The Earth Sciences*, edited by P. Lapointe and C. Barton, pp. 89-105, Plenum, New York.

Power, W. L., T. E. Tullis, S. R. Brown, G. N. Boitnott, and C. H. Scholz (1987), Roughness of natural fault surfaces, *Geophys. Res. Lett*, *14*, 29-32.

Power, W. L., T. E. Tullis, and J. D. Weeks (1988), Roughness and wear during brittle faulting, *Jour. Geophys. Res*, *93*(B12), 15,268-215,278.

Rempel, A. W., and J. R. Rice (2006), Thermal pressurization and onset of melting in fault zones, *Journal of Geophysical Research-Solid Earth*, *111*(B9), B09314, doi:09310.01029/02006JB004314.

Rice, J. R. (2006), Heating and weakening of faults during earthquake slip, *Journal of Geophysical Research-Solid Earth*, *111*(B5), doi:10.1029/2005JB004006.

Rice, J. R., and M. Cocco (2007), Seismic fault rheology and earthquake dynamics, in *The Dynamics of Fault Zones*, edited by M. R. Handy, p. in press, MIT Press, Cambridge, Mass.

Rice, J. R., E. M. Dunham, and H. Noda (2010), Thermo- and hydro-mechanical processes along faults during rapid slip, in *Meso-Scale Shear Physics in Earthquake and Landslide Mechanics*, edited by Y. Hatzor, J. Sulem and I. Vardoulakis, pp. 3-16, CRC Press.

Sagy, A., E. E. Brodsky, and G. J. Axen (2007), Evolution of fault-surface roughness with slip, *Geology*, *35*, 283-286, doi: 210.1130/G23235A.23231.

Schmitt, S. V., and P. Segall (2009), Thermal pressurization during "slip law" frictional earthquake nucleation, *Poster, 2009 SCEC Annual Meeting*.

Segall, P., and J. R. Rice (1995), Dilatancy, compaction, and slip instability of a fluid infiltrated fault, *J. Geophys. Res.*, *100*, 22155-22173.

Segall, P., and J. R. Rice (2006), Does shear heating of pore fluid contribute to earthquake nucleation?, *Journal of Geophysical Research-Solid Earth*, *111 (B09316)*, doi:10.1029/2005JB004129.

Sibson, R. H. (1973), Interactions between temperature and fluid pressure during earthquake faulting - A mechanism for partial or total stress relief, *Nature*, *243*, 66-68.

Thom, C. A., E. E. Brodsky, R. W. Carpick, G. M. Pharr, W. C. Oliver, and D. L. Goldsby (2017), Nanoscale roughness of natural fault surfaces controlled by scale-dependent yield strength, *Geophys. Res. Let.*, *44*, 9299-9307. doi:9210.1002/2017GL074663.